Preprint Title	Optimizing PMMA solutions to suppress contamination in the transfer of CVD graphene for batch production
Authors	Chun-Da Liao, Andrea Capasso, Tiago Queirós, Telma Domingues, Fatima Cerqueira, Nicoleta Nicoara, Jérôme Borme, Paulo Freitas and Pedro Alpuim
Publication Date	01 Jun 2022
Article Type	Full Research Paper
Supporting Information File 1	Capasso_BJN_SI.pdf; 820.6 KB
ORCID® iDs	Andrea Capasso - https://orcid.org/0000-0003-0299-6764; Tiago Queirós - https://orcid.org/0000-0001-6765-7793; Pedro Alpuim - https://orcid.org/0000-0001-9875-6188

Optimizing PMMA solutions to suppress contamination in the transfer of CVD graphene for batch production

Chun-Da Liao[a], *Andrea Capasso*[a,*], *Tiago Queirós*[a,b], *Telma Domingues*[a,b], *Fatima Cerqueira*[b], *Nicoleta Nicoara*[a], *Jérôme Borme*[a], *Paulo Freitas*[a], *Pedro Alpuim*[a,b,*]

[a] International Iberian Nanotechnology Laboratory, Braga 4715-330, Portugal

[b] Centro de Física das Universidades do Minho e Porto (CF-UM-UP), Universidade do Minho, Braga 4710-057, Portugal

Abstract: The mass production and consequent commercial adoption of graphene-based devices is still held back by a few crucial technical challenges related to quality control. In the case of graphene produced by chemical vapor deposition (CVD), the transfer process represents a delicate step that can compromise device performance, thus hindering industrial production. In this context, the impact of poly(methyl methacrylate) (PMMA) – the most common support material for transferring graphene from the Cu substrate to any target surface – can be decisive in obtaining reproducible sample batches. Although effective in mechanically supporting graphene during the transfer, PMMA solutions needs to be efficiently designed, deposited, and post-treated to serve their purpose while minimizing potential contaminations. Here, we prepared and tested PMMA solutions with different average molecular weight (AWM) and weight concentration in anisole, to be deposited by spin coating. Optical microscopy and Raman spectroscopy showed that the amount of PMMA residues on transferred graphene is proportional to the AMW and concentration in the solvent. Meanwhile, the mechanical strength of the PMMA layer resulted proportional to the AMW. These tests served to design an optimized PMMA solution made of a mixture of 550k and 15k AMW PMMA in anisole at 3% concentration. In this design, PMMA-550k provided a suitable mechanical strength against breakage during the transfer cycles, while PMMA-15k promoted de-polymerization which allowed a complete removal of PMMA residues without the need for any post-treatment. An XPS analysis

[*] Corresponding authors: andrea.capasso@inl.int, pedro.alpuim.us@inl.int

confirmed the cleanness of the optimized process. We validated the impact of the optimized PMMA solution in the mass-fabrication of arrays of electrolyte graphene field effect transistors operating as biosensors. On average, the transistor channel resistance decreased from 1860 Ω to 690 Ω when using the optimized PMMA. Even more importantly, the vast majority of these resistance values are distributed within a narrow range (only ~300 Ω wide), in evident contrast with the scattered values obtained in non-optimized devices (~30% showed values above 1 MΩ). These results prove that the optimized PMMA solution unlock the production of reproducible electronic devices over batch scale, key towards an industrial production.

Keywords: 2D materials, poly(methyl methacrylate), graphene transfer process, large-scale fabrication, microelectronics

Introduction

Graphene and two-dimensional (2D) transition metal dichalcogenides (TMDCs) have been the focus of an intense research effort aimed at developing a new class of innovative devices and applications [1–3]. Among the production methods, chemical vapor deposition (CVD) made substantial progress over the years and now guarantees high-quality standards for the growth of batches of graphene samples over wafer-scale areas [4–6]. This progress allowed the fabrication of a wide range of 2D material-based devices and heterostructures, especially in optoelectronics [7–9]. At present, one of the remaining challenges in the fabrication of graphene-based devices lies in the reproducibility: More than the CVD itself, the transfer process from the growth substrate (*e.g.*, Cu and Ni) to the desired target substrate (*e.g.*, SiO_2/Si, glass, flexible polymers, etc.) often introduce inconsistencies among devices. Various approaches have been developed to address this issue and establish a reproducible transfer process [10–16]. Among the many, the poly(methyl methacrylate) (PMMA)-assisted process remains the most reliable and used approach. The chemical structure of PMMA features long polymer chains, whose length is proportional to the average molecular weight (AMW) of the polymer. In the transfer of graphene, the polymer serves as a supporting layer to i) retain the integrity of graphene during the wet-etching bath required to dissolve the metallic substrate and ii) provide mechanical stability when transferring graphene to the target substrates. During this process, two primary external sources of contamination need to be considered: i) metallic particles from the Cu or Ni etching process; ii) PMMA residues after the removal and rinsing processes. Both contaminations are one of the leading

causes of undesired p-type doping in CVD graphene, accompanied by a deterioration of its electrical properties [17–20]. The metallic contamination from etchants such as $FeCl_3$ can be substantially reduced by rinsing PMMA-coated graphene in DI water solution with 1-2% HCl [11]. Concerning the PMMA residues, several approaches were implemented to dissolve them, primarily by disrupting their chemical bonds. The chemical bonding breakage is crucial when considering that PMMA solutions with higher weight percent (wt%) are usually preferred as they form thicker supporting layers by spin coating: Such layers are more mechanically robust yet leave behind significant residues [18]. Annealing processes (usually 200-450^{o}C, under an inert atmosphere or vacuum) [18]were proposed, enabling de-polymerization by breaking the molecular backbone bonds of PMMA [17,20,21]. Similarly, UV radiation can break the ester groups of PMMA, thus weakening the intermolecular interactions with graphene [22].

PMMA with higher AMW is harder to de-polymerize due to strong van der Waals and London attractive forces among the long polymeric chains [12]. It must also be considered that thermal treatments can often be counterproductive as they intensify polymerization, harden the PMMA residues, and complicate the removal. Therefore, the way toward clean graphene processing appears to lie in optimizing the PMMA-assisted processing. In this context, we propose an optimized approach for a clean mass transfer of graphene samples over wafer scales. A PMMA mixture was developed by balancing the AMW and wt% (ideally should both be as low as possible) in anisole, guaranteeing successful transfer and minimal contamination without post-treatment at high temperature. The supporting layer formed by spin coating presents high mechanical flexibility and strength for the transfer process and appears easy to dissolve afterward. We validated the impact of the optimized process in the mass fabrication of arrays of receded-gate graphene field-effect transistors for biosensing applications.

Results and discussion

We transferred graphene by using PMMA with two AMWs (15k and 550k), which were dissolved in anisole at two weight ratios (2 and 4 wt%). PMMA with 950k AMW (at 4%), commonly used for microfabrication processes as an e-beam resist, was used for further comparison (see the Experimental section, paragraph 2.2). Optical microscopy analysis was carried out to visually evaluate the presence of PMMA residues after the transfer process of graphene single crystals using PMMA at different wt% and AMW (Figure 1a-g). As detailed in the description of the graphene transfer process, after the Cu etching process (Figure S1b, step II), the PMMA-coated graphene is

rinsed in a DI water bath at least three times (Figure S1b, step III). Each cycle includes two actions, *i.e.*, (1) scooping up the sample and (2) releasing it into the water bath. After the rinse process, the sample must be moved to a target substrate, which takes one more transfer cycle. Therefore, the wet transfer process entails at least four cycles. A sufficiently high mechanical strength of the PMMA supporting layer is the key requirement for a successful transfer. Figure 1h shows our experimental observations on the cleanness level and max transfer cycles afforded by each PMMA solution. For statistical purposes, the number of cycles for each test was extended to eight by transferring the PMMA/graphene between two aqueous solutions. The PMMA solutions that allowed less than four cycles demonstrated low mechanical strength, such as A1 and C1 PMMA. The strength reached a proper level for A3 PMMA, which allowed up to six complete cycles. C3 and C4 PMMA provided the highest mechanical support, allowing up to ten cycles. To evaluate the process cleanness, the residues were quantified by counting the white spots (> 2.5 μm in size) in the images. Micrographs taken on 650×500 μm^2 areas were compared (Figure 1a-f). The amount of PMMA residues appears directly related to the PMMA concentration. A1 showed very low residues and low mechanical strength (they can be almost completely removed in acetone), while C1 provided proper support keeping a low residue level. The length of the PMMA molecular chain (proportional to molecular weight and the attractive intermolecular force) appeared to be the determining factor in the mechanical strength (as demonstrated by C3 PMMA, enabling 8 complete transfer cycles). Overall, all 550k samples provided strong mechanical support yet translated into a moderate-high residue density level. C4 revealed the densest residue distribution due to extended molecular chains and the highest mass concentration.

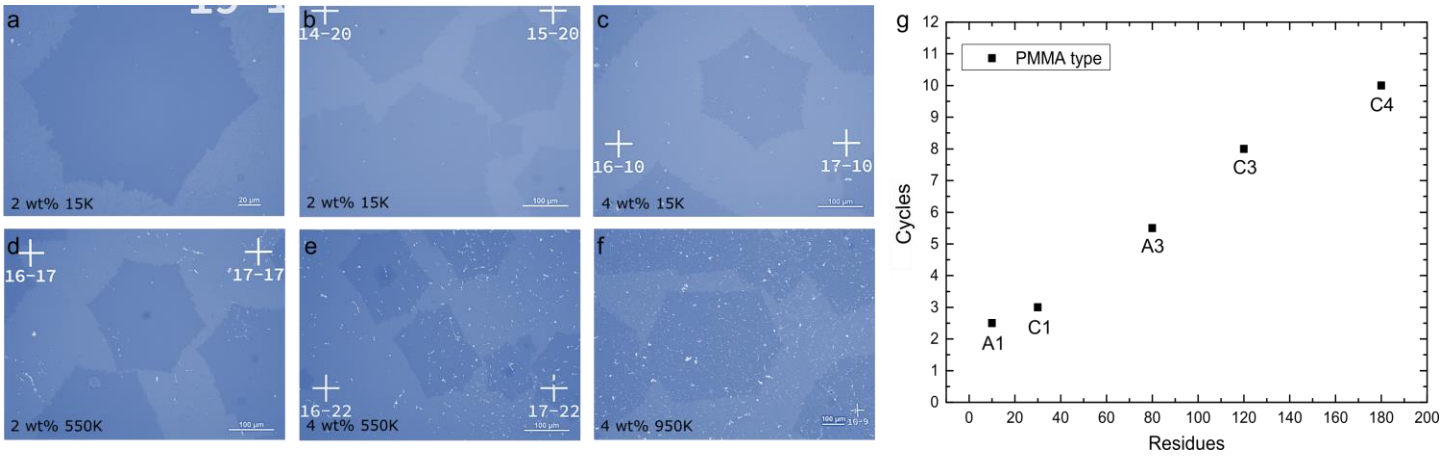

Figure 1. *Examination of PMMA residues after the transfer of graphene single crystals using PMMA at various wt% and AMW: a-b) A1, c) C1, d) A3, e) C3, f) C4. The white spots in the images are PMMA residues. The cross*

markers with coordinates are imprinted on the wafer to locate the graphene crystals. g) Number of residue particles spotted for different molecular weight PMMA.

A PMMA mixture (coded B2, 3% mixture of PMMA-15k and PMMA-550k, see Experimental section) was designed to lower the potential residue concentration while retaining proper mechanical support. The rationale for the design of the optimized mixture was based on two hypotheses: i) The PMMA-15k component provides short polymeric chains, which are expected to diminish the molecular chain entanglement, and hence the residue level. ii) The sole presence of short polymeric chains should, however, weaken the mechanical strength of the spin-coated layer. Therefore, the addition of PMMA-550k compensates for that and grants support during the transfer. B2 was tested in the transfer of both a graphene film and a single crystal (Figure 2a, b). The area analysis (650 × 500 μm^2) revealed only <10 residues, indicating an extremely clean transfer process. B2 PMMA allowed up to six transfer cycles, representing an intermediate yet acceptable mechanical support. It proves that the PMMA mixture features good mechanical strength and cleanness (*i.e.*, the acetone bath can thoroughly remove it). The transferred graphene samples were investigated via Raman spectroscopy to evaluate crystallinity, layer number, and structural defect level[21]. The relative intensities of G (∼1585 cm^{-1}) and 2D (∼2700 cm^{-1}) bands are typical of monolayer graphene[21–24]. The defect density appears minimal considering the negligible D-band intensity at ∼1350 cm^{-1} (Figure 2c)[25]. The Raman mapping in Figure 2d-i examines the whole crystal area [26]. The map and corresponding statistics in Figures 2d and g show that the I(D)/I(G) is very low (down to 0.03), meaning that no or few defects could be detected. Figures 2e and h show that over 95% of the sample has I(2D)/I(G)>1.6 (average of 2.1 ± 0.3) and a FWHM (2D) of 34.2 ± 3.0 cm^{-1} (Figure 2f and i), implying high-quality monolayer graphene. Together, the data further support the sample uniformity and crystallinity.

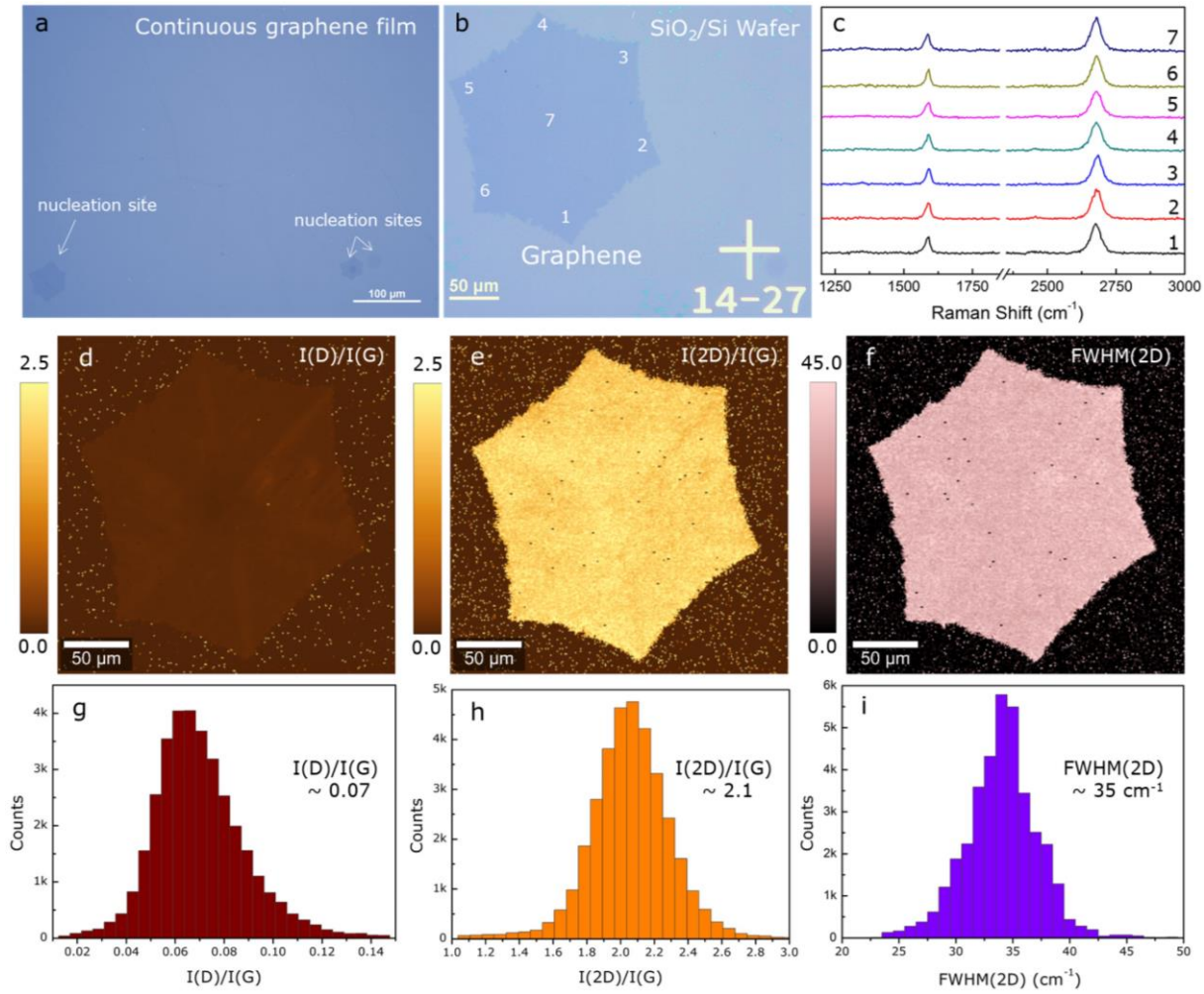

Figure 2. *Raman analysis of graphene samples transferred with the optimized B2 PMMA. Optical images of (a) a large-area film and (b) a single crystal. (c) Raman spectra taken in the positions indicated in (b). Raman mapping of (d) I(D)/I(G), (e) I(2D)/I(G) and (f) FWHM(2D), and (g-i) corresponding statistics.*

The G phonon band arises from double degeneracy of iTO and iLO phonon mode (E_{2g} symmetry) at the Brillouin zone center, which is an in-plane vibration of sp^2 carbon atoms[21], and its position displays a blue shift as the charge carrier concentration rises, *i.e.*, the frequency shift of the G band is proportional to $|E_F|$, which sets the carrier concentration. Due to the method and materials employed for the graphene transfer being the same except for the PMMA mixture, we consider that the differences in Raman spectra between the various samples can be attributed to adsorbed PMMA residues. Such residues could absorb water and oxygen molecules, conferring p-type doping to graphene[27]. Conversely, by tracking the G phonon band features in Raman spectra, we can correlate the degree of doping in graphene[28,29] with PMMA residues. A comparison of the statistical data of the G band position and

FWHM(G) of graphene transferred with C4 and B2 PMMA is presented in Figure 3. Representative Raman spectra for the two cases are shown in Figures 3a and b). The comparison of Figures 3c and d shows that the G peak position is blue-shifted in C4 samples concerning B2 ones (from an average of 1587 to 1593 cm^{-1}), indicating that the charge carrier concentration did not rise as much when using the B2 PMMA, which shows that B2 leaves behind a much lower (if any) density of residues. This red shift observed upon reducing the PMMA residue concentration is consistent with studies on advanced methods for cleaning PMMA from graphene[30]. The average FWHM(G) for the C4 and B2 samples is ~14 and 23 cm^{-1}, respectively (Figures 3e and f). The broader G phonon band observed for the B2 samples reveals that a more significant number of inter-band decay pathways are available due to a lower Pauli blocking threshold[21] (equivalent to twice $|E_F|$), further indicating that the p-type doping caused by adsorbed PMMA is less intense for the B2 samples. This result again supports that employing the B2 PMMA yields fewer residues and may assist in avoiding post-transfer treatments for advanced PMMA residue cleaning of graphene, such as annealing and ion beam irradiation[30]. The graph of the G-band shift (Figure S2a) confirms that C4 PMMA leaves the highest level of contamination. This case also shows the highest standard variation of the G-band shift and FWHM (G) (Figures S2a and b) due to heterogeneous doping levels in the sample. We explain these results by the higher variance in the proportions of PMMA residue aggregates, resulting in alternating regions of intensively local p-type doping (large PMMA aggregates) and regions of less intense p-doping (small PMMA aggregates). In contrast, lighted molecular weight and AMW PMMA-mixtures showed lighter and more uniform p-type doping over the crystallite area (smaller error bars). Few-layer crystals transferred with B2 are analyzed in Figure S3. The graphene crystal in Figure S3a, b is composed of four layers having a thickness of 0.4-0.5 nm (Figure S3c)[26,31]. The crystal morphology appears very smooth and free of identifiable impurities, with an average surface roughness (R_a) of ~0.2 nm (figure S3d). This value is more than one order of magnitude lower than that of graphene crystals transferred with C4.

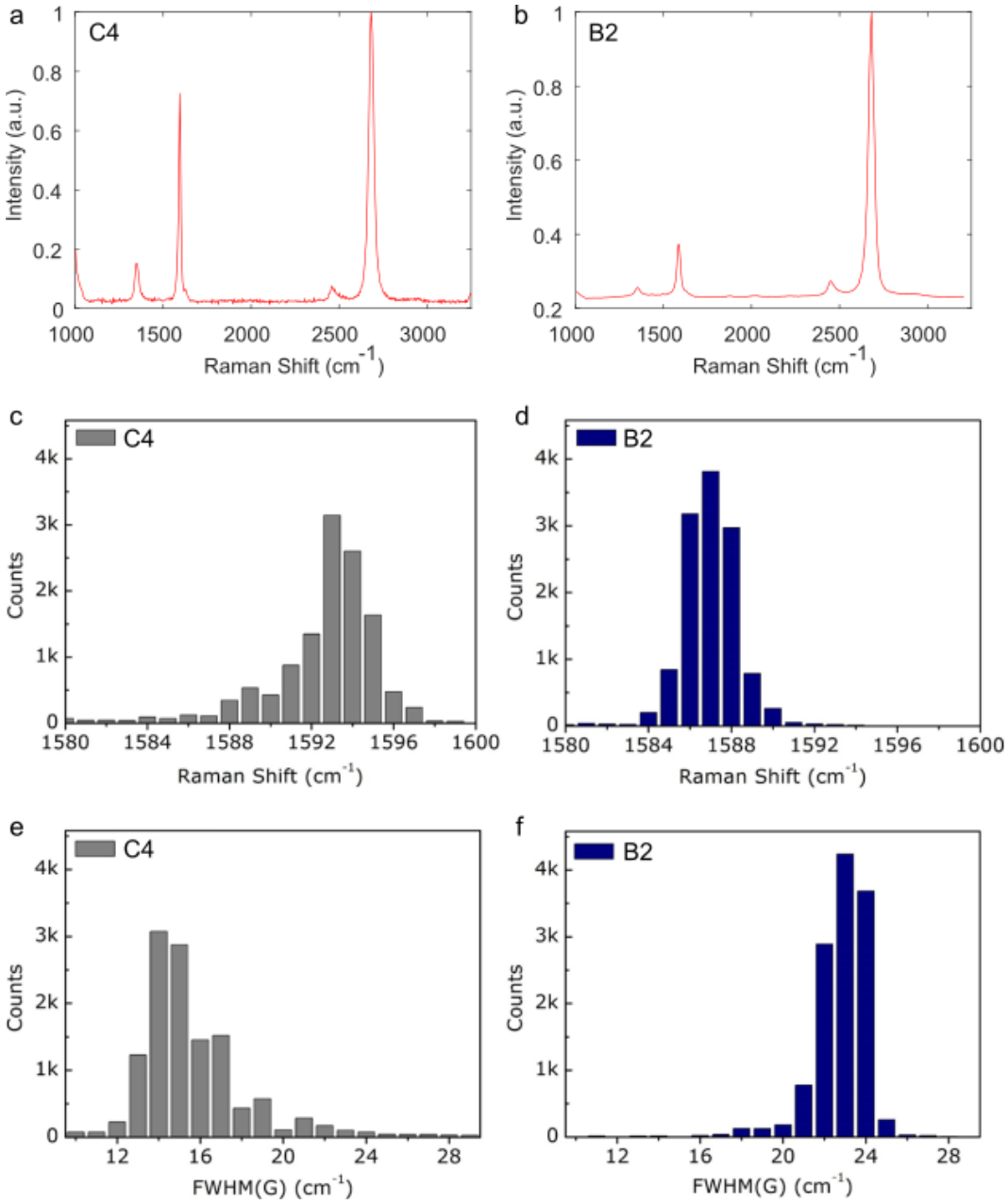

Figure 3. *Statistical analysis of the Raman spectra of transistors prepared with transfers using different molecular weight PMMA mixtures. (a, b) Representative Raman spectra of graphene transistor channels prepared using B2 and C4 mixtures, respectively. (c, d) Distributions of the G band peak position for B2 and C4. (e, f) Distributions of the FWHM of the G band.*

XPS was employed to analyze the graphene samples transferred by C4 and B2 PMMA (Figure 4). Figure 4a shows the chemical structure of the PMMA molecule. The C1s spectra can be decomposed into two prominent peaks, originating from sp^2 hybridized C–C and sp^3 hybridized C–C/C–H bonds. Four PMMA-related peaks can be

assigned to C–H, C–C, O–CH_3 (methoxy functional group), and O–C=O (carboxyl functional group) bonds, respectively[32–34]. PMMA residues on graphene surface mainly feature three peaks resulting from C–C bonds and carbon-oxygen-related bonds (*i.e.*, methoxy and carboxyl functional groups). After PMMA was cleaned in the acetone bath, the peak of the C–H bond can rarely be observed because of a broader merger with the peak of sp^3 hybridized C–C/C–H bond in graphene. In Figure 4b, the peak intensities of C–C, O–CH_3, and O–C=O bonds are 17.6, 14.6, and 15.0% of the main peak intensity (sp^2 C–C). In Figure 4c, the same respective ratios decrease to 2.9, 2.6, and 4.8%. Therefore, regarding O–C=O bonds, the residue caused by B2 was reduced by 3 times and decreased about 6 times for the removal of C–C and O–CH_3 bonds, implying the crucial role of PMMA-15k in the mixture.

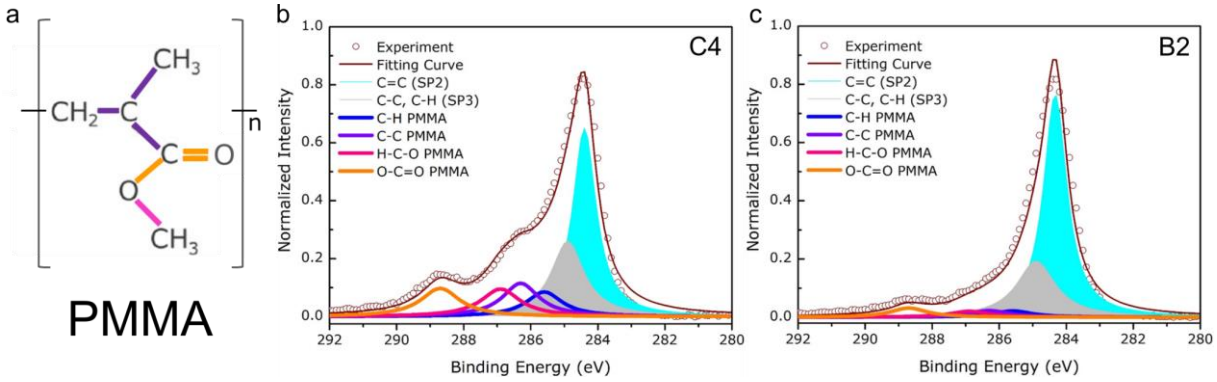

Figure 4. *(a) Representation of PMMA's molecular structure. XPS C1s spectra of graphene samples transferred using (b) C4 and (c) B2. The normalized spectra are fitted by Gaussian-Lorentzian curves. The solid blue and grey fill identify sp^2 and sp^3 hybridized carbon bonds in graphene, located at ~284.4 and 285.0 eV, respectively. C–H (blue line), C–C (purple line), O–CH_3 (pink line), and O–C=O (orange line) bonds are located at ~285.7, 286.3, 287.0 and 289.0 eV, respectively.*

The optimized graphene transfer process was statistically validated in a batch fabrication context by comparing the channel resistance of graphene-based EGFETs (Figure 5) designed to operate as electrolyte graphene-based DNA biosensors. Two batches of EGFETs having a topmost graphene channel (75 µm width × 25 µm length) were fabricated (see details in SI). In the first batch[35,36] (including 1755 EGFETs), graphene was transferred with C4 PMMA mixture (see Section 0). The data acquired from the first batch were used to benchmark a successive test on a more extensive second batch[37,38] (4200 EGFETs) that used B2 PMMA for the graphene transfer. Figure

5 shows the resistance distribution in the two cases. The distributions were fitted with multiple Gaussian curves to identify the predominant resistance values in each transistor batch. The C4 and B2 first Gaussian curves (which envelop the most common resistance bins, see Figure 5) peak at 1860 and 690 Ω, respectively – *i.e.*, a difference of 1170 Ω. The much lower channel resistance for B2 mixture gives further evidence of a more robust, cleaner, and effective transfer process. The B2 transfer appears to minimize the PMMA residues, known to act as centers of carrier scattering in graphene and increase its resistance[17,18]. The vast majority (~90%) of B2 data populate the first Gaussian curve, with a narrow distribution (FWHM of ~300 Ω). By stark contrast, the C4 data are scattered over a much broader range: almost 50% populate a broader Gaussian curve with two peaks (first peak FWHM ~567 Ω) in the range up to 15 kΩ, while more than 20% have values up to 1 MΩ. Differently from B2, a consistent sample subset (above 30%) is above 1 MΩ, which means that a third of the fabricated devices are open circuits due to an imperfect graphene transfer (leading to highly damaged or lacking graphene). Overall, the B2 mixture yields more consistent electric properties of the graphene channel, thanks to a homogenous and reproducible process. Such characteristics ultimately translate into a consistent sensor performance, which is pivotal for industrial fabrication.

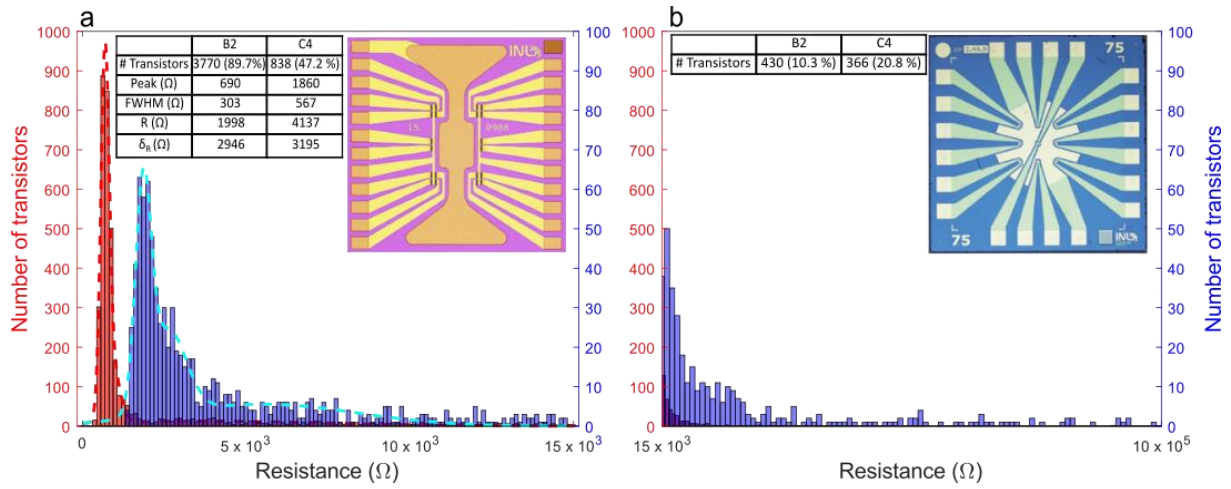

***Figure 5**: Distributions of the graphene channel resistance values in devices made by C4 (blue) and B2 (red) PMMA. The top-right corner of each panel contains an optical micrograph of representative B2 (left) and C4 (right) transistors. The graphs show the resistance distributions in a) 0-15 kΩ range (with 125 Ω bins); b) 15 kΩ-1 MΩ range (10 kΩ bins). The multiple Gaussian fittings identify the dominant resistance values in both batches.*

Likewise, when considering all the sub-15000 Ω transistors, the difference between average resistances is 2139 Ω.

Conclusion

Monolayer graphene films and single crystals were transferred using PMMA with different AMW and wt% in anisole. The repeated transfer cycles among water baths revealed, as expected, that PMMA at higher AMW and wt% allowed higher mechanical support to graphene. Optical microscopy, Raman spectroscopy, and XPS results carried out to evaluate the amount of PMMA residues on graphene after the transfer processes showed that PMMA with higher AMW resulted in a more significant number of residues: PMMA-950k AMW (C4) yielded a maximum 180 residues (in a 650 × 500 μm^2 area), while the optimized mixture (PMMA-15k/550k – B2) yield a minimum value of 10 residues in the same area. More abundant PMMA contamination on graphene translated into a more intense p-type doping, as evidenced by i) the position of the Raman G peak, which blue-shifted by ~6 cm^{-1} (between C4 and B2 samples), and ii) the FWHM of the G peak, which appeared broader in B2 samples (23 cm^{-1} *vs* 14 cm^{-1} of the C4 samples). The XPS analysis showed a much-increased presence of C–H, C–C, O–CH_3, and O–C=O bonds in C4 graphene compared to B2 samples, corroborating the previous findings. We validated the impact of the optimized B2 process in the mass fabrication of arrays of electrolyte-gated graphene field-effect transistors (EGFETs). The channel resistances of thousands of EGFETs prepared using B2, and C4 PMMA were measured with a probe station in air. The resistance distributions were analyzed and fitted with Gaussian curves. The resistance distributions were centered at 690 Ω (FWHM= 303 Ω) and 1860 Ω (FWHM=567 Ω), respectively, proving that the optimized PMMA mixture enables the production of reproducible arrays of electronic devices with consistent properties.

Experimental

Graphene growth

Single-crystal and large-area graphene were obtained on Cu foil via catalyst-assisted growth in a low-pressure CVD system (CVD First Nano, EasyTube 3000). A 25-µm-thick annealed Cu foil (Alfa Aesar, purity 99.8%), serving as a metal catalyst, was placed in a graphite enclosed cavity during the whole process. The temperature

for annealing and growth was kept stable at 1040 °C by PID thermal controllers. The Cu foil was first annealed in argon atmosphere (500 sccm, 9.0 torr) for 30 min in the quartz tube furnace. In the growth process, the gas mixture of argon (250 sccm), hydrogen (100 sccm), and methane (1.2 sccm) was subsequently introduced into the quartz chamber, where reaction pressure of 4.0 torr was kept constant through the variable frequency-driven pumping system. The growth time for single graphene crystals (250 – 350 μm) and large-area graphene films (~ 25 cm^2) was 40 min and 80 min, respectively. To finalize the process, an argon flush of 500 sccm was conducted to cool down samples until the furnace reached room temperature.

Graphene transfer

For the preparation of the various PMMA solutions, PMMA-15k (Sigma-Aldrich, 200336) and PMMA-550k (Alfa Aesar, 43982) powders were dissolved in anisole (Merck, 801452) in different proportions, as indicated in Table 1. PMMA-950K (MicroChem, PMMA-950k A4) at 4 wt% is commonly used for microfabrication processes and was chosen for comparison. The optimized PMMA mixture (coded B2) was made by mixing PMMA-550k and PMMA-15k in anisole at a 2:1 ratio (3 wt%). The solutions were stirred at 1000 rpm for 24 hours. The graphene transfer process is illustrated in Figure S1. Graphene/Cu foil was spin-coated with PMMA at 3000 rpm for 30 sec, followed by drying in a fume hood for 8 h. The backside graphene was removed by oxygen plasma (4 x 10^{-1} mbar, 250 W, 90 seconds).

Table 1: PMMA solutions used in the graphene transfer tests.

Name	Ratio (wt %)	Polymer AMW	Polymer wt% (g)	Anisole wt (g)
A1	2%	15k	2	98
C1	4%	15k	4	96
A3	2%	550k	2	98
C3	4%	550k	4	96
C4	4%	950k	4	96
B2	3%	15k / 550k	1 / 2	97

PMMA/graphene/Cu foil was placed over the 0.5 M $FeCl_3$ solution surface for 3 h to etch away the Cu foil. After the etching process, PMMA/graphene floating on the surface of the $FeCl_3$ solution was rinsed with DI water three times. A rinse in 2% HCl solution was done to remove metal precipitates. At last, the PMMA/graphene was washed

in DI water three times and scooped up with a target substrate (SiO_2/Si wafer). The sample was dried in a vacuum chamber (~10^{-4} Torr) at room temperature for 2 h. For PMMA removal, the entire sample was vertically dipped into an acetone bath for 4 h. After that, the exposed graphene on a SiO_2/Si substrate was again vertically dipped into IPA and then DI water bath for 1 hr. Finally, the graphene on the receiving substrate was blow-dried with N_2.

Optical microscopy

The selective oxidation method was adopted to rapidly identify the as-grown graphene, enabling the direct optical inspection of the graphene domains without the laborious transfer process. Following this method, the Cu substrate with graphene was first oxidized in ambient air on a hot plate at 200^{o}C for 2 min. The graphene film on the Cu substrate serves as a protection layer, preventing the underlying Cu surface from oxidation because of its high chemical/thermal stability and impermeability to gases and liquids. In contrast, the surrounding exposed areas of the Cu foil surface exhibited high reactivity and were readily oxidized to copper oxides with a noticeable color change. The apparent color contrast between the oxidized and non-oxidized Cu surfaces made the synthesized graphene domains easy to be observed in an optical microscope equipped with a CCD camera (Figure S1a).

Raman spectroscopy

Large-area graphene films and single graphene crystals transferred onto SiO_2/Si substrates were characterized by Raman microscopy (WITec GmbH, Model: Alpha300M+) with an excitation laser line of 532 nm. The laser power of ~2 mW was used for all measurements. The backscattered laser light containing the Raman bands from 1200 to 3000 cm^{-1} was collected by a CCD camera (Andor, Model number: DV401A-BV-352) integrated with the WITec system. The characteristic Raman signature collected from a *p*-doped Si wafer at 520.7 cm^{-1} was employed as standard calibration. Raman mapping was conducted by raster scan, where the step size of the laser spot moving over a selected area is 1 μm, and the exposure time of 0.4 s was taken at each point of the mapping. In the maps, the intensity of D and 2D bands were normalized to the G band intensity. Corresponding statistics were extracted from the maps.

X-ray Photoelectron Spectroscopy

The chemical components of PMMA residues were analyzed by X-ray photoelectron spectroscopy (XPS, Thermo Scientific ESCALAB 250Xi) using a non-monochromatic Mg Kα source with an analysis spot of < 2 mm^2. The Detection system equips a double-focusing 180º spherical sector analyzer with a mean radius of 150 mm and an energy range of 0 to 5 keV. The pressure in the analysis chamber was ~ 5 x 10^{-10} Torr, and the analyzer had a pass energy of 20 eV.

Atomic Force Microscopy

The surface topographies of graphene were investigated by Bruker Dimension Icon atomic force microscopy (AFM), using PPP-NCH (NanosensorsTM) cantilevers with a tip radius of < 20 nm, force constant of 42 N/m, and 250 kHz resonance frequency. The AFM measurement was carried out in tapping mode. A 633-nm laser light aimed at the backside of the cantilever tip was reflected toward a position-sensitive photodetector, which provides feedback signals to piezoelectric scanners that maintain the cantilever tip at constant height (force) above the surface, thus reproducing its topography.

Graphene-based Field Effect Transistor Fabrication and Characterization

Receded-gate graphene field-effect transistors (GFETs) were fabricated on 8" Si/SiO_2 (200 nm thick) wafers. Two arrays of devices were fabricated with different process steps (Wafer 1 - C4 PMMA; Wafer 2 – B2 PMMA). Both wafers started with the patterning of Cr/Au contacts (deposited by magnetron sputtering) using direct-write laser lithography and ion milling. The fabrication of the two wafers followed slightly different steps, as described below.

Wafer 1: A stopping layer (Al_2O_3/TiWN/AlSiCu/TiWN) was patterned by lift-off, followed by the CVD growth of a multi-stack layer of SiO_2 and Si_3N_4 to passivate the current lines. After this, a thin Al_2O_3 layer was deposited by sputtering and patterned by wet etching to protect the gate during the graphene etch. The C4 PMMA/graphene films were then transferred onto the patterned wafer until all device areas were covered. After removing the PMMA, graphene was patterned using optical lithography and oxygen plasma etching. Finally, the sacrificial layer was removed by wet etching.

Wafer 2: An additional layer of Al_2O_3 was deposited on the Au layer as protection. After that, the two wafers followed different fabrication processes. A residue-free transfer process was used, using a sacrificial metallic mask

(TiWN, AlSiCu, TiWN) patterned by lift-off to protect the entire wafer except for the areas around the channel, source, and drain, on which the graphene film would make electrical contact. The B2 PMMA/Graphene films were then transferred onto the wafer and patterned by O_2 plasma, followed by the sacrificial layer removal. Previously to the passivation, Al_2O_3 was selectively removed to improve the adhesion of the oxide passivation to the chips' surface. A stopping layer (Cu/AlSiCu/TiW) for the reactive ion etching (RIE) process was sputtered, and the SiO_2/SiN_x multi-stack passivation layer was deposited by CVD. The passivation layer was patterned by lithography and etched by RIE until revealing the stopping layer on the contact pads and graphene transistor channels. Finally, the stopping layer was removed by wet etching, exposing the graphene channel.

In both wafers, the GFET channels had nominal dimensions W = 75 µm and L = 25 µm. The total number of GFETs condidered in this study was 1755 on Wafer 1 and 4200 on Wafer 2. The source-drain resistance of the GFETs was measured with a semi-automatic DC measurement probe station for 8" wafers. The setup uses a 40-tips probe head with 250 µm spacing among tips; each probe allowed it to measure 20 devices simultaneously. A current was injected into each transistor to reach an output voltage of 1 mV. Histogram distributions for the graphene channel resistances were plotted (using MATLAB scripts) to compare the effects of B2 and C4 PMMA-assisted graphene transfer on device performance. Based on our observations of the device performance, a threshold resistance of 15000 Ω was selected as the cut-off resistance value identifying working graphene channels (*i.e.*, correctly operating devices). A maximum resistance value of 1 MΩ was set to identify the non-operating channels (due to imperfect transfer leading to heavily damaged or lacking graphene). Multiple Gaussian fits were performed to isolate the trends in the resistance distributions.

Funding

We acknowledge the financial support of the project "GEMIS – Graphene-enhanced Electro-Magnetic Interference Shielding", with the reference POCI-01-0247-FEDER-045939, co-funded by COMPETE 2020 – Operational Programme for Competitiveness and Internationalization and the Portuguese Foundation for Science and Technology (FCT), under the Portugal 2020 Partnership Agreement, through the European Regional Development Fund (ERDF) and the FCT via the Strategic Funding UIDB/04650/2020. C.D. Liao acknowledges a Marie Skłodowska-Curie COFUND Fellowship (H2020-MSCA-COFUND 2015). T.Queirós acknowledges a PhD grant

from FCT with reference SFRH/BD/150646/2020 in the framework of the Quantum Portugal Initiative. T. Domingues acknowledges a PhD grant from FCT with reference SFRH/BD/08181/2020.

References

1. Butler, S. Z. *et al.* Progress, challenges, and opportunities in two-dimensional materials beyond graphene. *ACS Nano* **7**, 2898–2926 (2013).

2. Geim, A. K. & Grigorieva, I. V. Van der Waals heterostructures. *Nature* **499**, 419 (2013).

3. Novoselov, K. S., Mishchenko, A., Carvalho, A. & Castro Neto, A. H. 2D materials and van der Waals heterostructures. *Science (80-.).* **353**, (2016).

4. Obraztsov, A. N. Chemical vapour deposition: making graphene on a large scale. *Nat. Nanotechnol.* **4**, 212 (2009).

5. Hao, Y. *et al.* The Role of Surface Oxygen in the Growth of Large Single-Crystal Graphene on Copper. *Science (80-.).* **342**, 720 LP-- 723 (2013).

6. Chen, C.-C. *et al.* Growth of large-area graphene single crystals in confined reaction space with diffusion-driven chemical vapor deposition. *Chem. Mater.* **27**, 6249–6258 (2015).

7. Han, T.-H. *et al.* Extremely efficient flexible organic light-emitting diodes with modified graphene anode. *Nat. Photonics* **6**, 105 (2012).

8. Britnell, L. *et al.* Strong light-matter interactions in heterostructures of atomically thin films. *Science (80-.).* **340**, 1311–1314 (2013).

9. Gomez De Arco, L. *et al.* Continuous, highly flexible, and transparent graphene films by chemical vapor deposition for organic photovoltaics. *ACS Nano* **4**, 2865–2873 (2010).

10. Liang, X. *et al.* Toward clean and crackless transfer of graphene. *ACS Nano* **5**, 9144–9153 (2011).

11. Kim, S. M. *et al.* The effect of copper pre-cleaning on graphene synthesis. *Nanotechnology* **24**, 365602 (2013).

12. Kim, S. *et al.* Robust graphene wet transfer process through low molecular weight polymethylmethacrylate. *Carbon N. Y.* **98**, 352–357 (2016).

13. Lin, Y.-C. *et al.* Graphene annealing: how clean can it be? *Nano Lett.* **12**, 414–419 (2011).

14. Barin, G. B. *et al.* Optimized graphene transfer: Influence of polymethylmethacrylate (PMMA) layer concentration and baking time on graphene final performance. *Carbon N. Y.* **84**, 82–90 (2015).

15. Capasso, A. *et al.* Cyclododecane as support material for clean and facile transfer of large-area few-layer graphene. *Appl. Phys. Lett.* **105**, 113101 (2014).

16. Ullah, S. *et al.* Graphene transfer methods: A review. *Nano Res.* **14**, 3756–3772 (2021).

17. Suk, J. W. *et al.* Enhancement of the electrical properties of graphene grown by chemical vapor deposition via controlling the effects of polymer residue. *Nano Lett.* **13**, 1462–1467 (2013).

18. Pirkle, A. *et al.* The effect of chemical residues on the physical and electrical properties of chemical vapor deposited graphene transferred to SiO2. *Appl. Phys. Lett.* **99**, (2011).

19. Ahn, Y., Kim, H., Kim, Y.-H., Yi, Y. & Kim, S.-I. Procedure of removing polymer residues and its influences on electronic and structural characteristics of graphene. *Appl. Phys. Lett.* **102**, 91602 (2013).

20. Jeong, H. J. *et al.* Improved transfer of chemical-vapor-deposited graphene through modification of intermolecular interactions and solubility of poly (methylmethacrylate) layers. *Carbon N. Y.* **66**, 612–618 (2014).

21. Malard, L. M., Pimenta, M. A., Dresselhaus, G. & Dresselhaus, M. S. Raman spectroscopy in graphene. *Phys. Rep.* **473**, 51–87 (2009).

22. Ferrari, A. C. & Basko, D. M. Raman spectroscopy as a versatile tool for studying the properties of graphene. *Nature Nanotechnology* (2013) doi:10.1038/nnano.2013.46.

23. Pimenta, M. A. *et al.* Studying disorder in graphite-based systems by Raman spectroscopy. *Phys. Chem. Chem. Phys.* **9**, 1276–1290 (2007).

24. Faggio, G. *et al.* High-Temperature Growth of Graphene Films on Copper Foils by Ethanol Chemical Vapor Deposition. *J. Phys. Chem. C* **117**, 21569–21576 (2013).

25. Lisi, N. *et al.* Rapid and highly efficient growth of graphene on copper by chemical vapor deposition of ethanol. *Thin Solid Films* **571**, 139–144 (2014).

26. Gnisci, A. *et al.* Ethanol-CVD Growth of Sub-mm Single-Crystal Graphene on Flat Cu Surfaces. *J. Phys. Chem. C* **122**, (2018).

27. Ni, Z. H. *et al.* The effect of vacuum annealing on graphene. *J. Raman Spectrosc. An Int. J. Orig. Work all Asp. Raman Spectrosc. Incl. High. Order Process. also Brillouin Rayleigh Scatt.* **41**, 479–483 (2010).

28. Das, A. *et al.* Monitoring dopants by Raman scattering in an electrochemically top-gated graphene transistor. *Nat. Nanotechnol.* **3**, 210 (2008).

29. Wu, J.-B., Lin, M.-L., Cong, X., Liu, H.-N. & Tan, P.-H. Raman spectroscopy of graphene-based materials and its applications in related devices. *Chem. Soc. Rev.* **47**, 1822–1873 (2018).

30. Zhuang, B., Li, S., Li, S. & Yin, J. Ways to eliminate PMMA residues on graphene —— superclean graphene. *Carbon N. Y.* **173**, 609–636 (2021).

31. Capasso, A. *et al.* Nitrogen-doped graphene films from chemical vapor deposition of pyridine: influence of process parameters on the electrical and optical properties. *Beilstein J. Nanotechnol.* **6**, 2028–2038 (2015).

32. Ton-That, C., Shard, A. G., Teare, D. O. H. & Bradley, R. H. XPS and AFM surface studies of solvent-cast PS/PMMA blends. *Polymer (Guildf).* **42**, 1121–1129 (2001).

33. Ferrah, D. *et al.* XPS investigations of graphene surface cleaning using H2-and Cl2-based inductively coupled plasma. *Surf. interface Anal.* **48**, 451–455 (2016).

34. Cunge, G. *et al.* Dry efficient cleaning of poly-methyl-methacrylate residues from graphene with high-density H2 and H2-N2 plasmas. *J. Appl. Phys.* **118**, 123302 (2015).

35. Campos, R. *et al.* Attomolar Label-Free Detection of DNA Hybridization with Electrolyte-Gated Graphene Field-Effect Transistors. *ACS Sensors* **4**, 286–293 (2019).

36. Filipa, C. & Abreu, M. Biosensors for enhanced in vitro fertilisation outcomes. (Swansea University, 2019).

37. Cabral, P. D. *et al.* Clean-room lithographical processes for the fabrication of graphene biosensors. *Materials (Basel).* **13**, 1–23 (2020).

38. Purwidyantri, A. *et al.* Influence of the Electrolyte Salt Concentration on DNA Detection with Graphene Transistors. (2021).